# The kinetic Alfvén-like nature of turbulent fluctuations in the Earth's magnetosheath: MMS measurement of the electron Alfvén ratio

(ID) O. W. Roberts, (ID) Y. Narita, (ID) R. Nakamura, et al.

**COLLECTIONS**

Paper published as part of the special topic on Plasma Physics from the Magnetospheric Multiscale Mission

View Online        Export Citation        CrossMark

---

**ARTICLES YOU MAY BE INTERESTED IN**

Turbulence-driven magnetic reconnection and the magnetic correlation length: Observations from Magnetospheric Multiscale in Earth's magnetosheath
Physics of Plasmas **29**, 012302 (2022); https://doi.org/10.1063/5.0071106

Statistical investigation of electric field fluctuations around the lower-hybrid frequency range at dipolarization fronts in the near-earth magnetotail
Physics of Plasmas **29**, 012111 (2022); https://doi.org/10.1063/5.0067382

Turbulence in space plasmas: Who needs it?
Physics of Plasmas **28**, 032306 (2021); https://doi.org/10.1063/5.0041540

# The kinetic Alfvén-like nature of turbulent fluctuations in the Earth's magnetosheath: MMS measurement of the electron Alfvén ratio

View Online          Export Citation          CrossMark

O. W. Roberts,[1,a)]  Y. Narita,[1]  R. Nakamura,[1]  Z. Vörös,[1,2]  and D. Verscharen[3]

## AFFILIATIONS

[1]Space Research Institute, Austrian Academy of Sciences, Graz 8010, Austria
[2]Institute of Earth Physics and Space Science, ELRN, Sopron 9400, Hungary
[3]Mullard Space Science Laboratory, University College London, Dorking RH5 6NT, United Kingdom

**Note:** This paper is a part of the Special Collection: Plasma Physics from the Magnetospheric Multiscale Mission.
[a)]Author to whom correspondence should be addressed: Owen.Roberts@oeaw.ac.at

## ABSTRACT

The Magnetospheric MultiScale (MMS) mission is used to investigate turbulent fluctuations in the Earth's magnetosheath. The unique combination of multiple spacecraft and high time resolution plasma and electromagnetic field data provided by MMS makes it an ideal mission to study the nature of turbulence and energy conversion. The multiple spacecraft allow the determination of the wavevector directions and plasma frame frequencies of the fluctuations. Moreover, the particle velocities allow the determination of the ion and electron Alfvén ratios, giving an additional diagnostic to reveal the nature of the turbulent fluctuations. Finally, the currents (determined from plasma moments) and the three-dimensional electric field measurements allow the determination of a scale-dependent energy conversion rate. The results reveal that the fluctuations predominantly have kinetic Alfvén wave-like properties at wavenumbers near $k\rho_i \sim 1$ (where $\rho_i$ is the ion gyroradius) and that Landau damping is an important pathway for converting energy.

*Published under an exclusive license by AIP Publishing.* https://doi.org/10.1063/5.0068828

## I. INTRODUCTION

Plasma turbulence is a ubiquitous process in the heliosphere. *In situ* observations in the solar wind[1–3] and planetary magnetosheaths[4–8] reveal disordered fluctuations in electromagnetic fields and particle velocities. Energy is deposited into the system at large scales before undergoing a fluid-like turbulent cascade with eddies and fluctuations transferring energy to smaller scales. At the scales smaller than the particle gyration scales or where the particles decouple from the magnetic field, energy can be transferred efficiently from the fields to the particles' bulk kinetic and internal energies.

The exact mechanism or mechanisms behind plasma heating and acceleration in heliospheric plasma are unclear. Possible explanations include damping of electromagnetic waves[9–11] and dissipation in coherent structures.[12,13] Several different types of waves and coherent structures can exist in plasmas. At the moment, it is not clear how they interact with one another,[14,15] and how they contribute to the observed heating and acceleration of particles. Identifying the nature of the fluctuations and comparing their polarization properties to

those known from simplifying models (such as linear solutions to the Vlasov equation) can aid our understanding.

This paper aims to use both the multi-spacecraft capabilities of Magnetospheric MultiScale (MMS) and the high time resolution of particle data to understand the nature of the fluctuations in the Earth's magnetosheath and compare them to the predictions for waves from the linear Vlasov theory. The particle measurements of the current density $\mathbf{J}$ can also allow us to investigate $\mathbf{J} \cdot \mathbf{E}'$ (where $\mathbf{E}'$ denotes the electric field after transformation into a particle frame, i.e., ions or electrons), which quantifies the conversion of energy between the fields and the kinetic energy.

## II. DATA/METHODOLOGY

On 2 September 2015, the MMS spacecraft[16] recorded an interval of Earth's magnetosheath in burst survey resolution. The spacecraft was located at [3.3, 11.4, −0.2] Re in the Geocentric Solar Ecliptic (GSE) coordinate system (where x points from Earth to the Sun and z points to the Solar ecliptic North). Magnetic field data were recorded

from the fluxgate magnetometers[17] at a rate of 128 Hz. Plasma data were measured by the Fast Plasma Investigation[18] with a sampling rate of 6.6 Hz for ions and 30.3 Hz for electrons. Electric field data were recorded from the spin plane double probes (SDP),[19] which measure the x and y GSE components, and the axial double probe (ADP),[20] which measures the z component. Together, the SDP and ADP give a measurement of the three dimensional electric field with a sampling rate of 8.192 kHz. An overview of the data from the MMS1 spacecraft during the analyzed time interval is presented in Fig. 1.

The four MMS spacecraft make a regular tetrahedron with low values of planarity and elongation;[21] P = 0.26 E = 0.12, respectively, and a mean inter-spacecraft distance of 140 km which is close to the ion's characteristic scales. This time interval occurred briefly after launch and was before MMS achieved its nominal separations of the order of tens of kilometers. The large formation is ideal for studying ion scale physics. The mean parameters (in GSE coordinates) are as follows: magnetic field B = [−15.2, 24.0, 41.1] nT, ion velocity [−214, 154, −109] km/s, electron velocity [−195, 144, −94] km/s. The measured ion density $n_i = 26.7$ cm$^{-3}$ and electron density $n_e = 27.1$ cm$^{-3}$ are almost identical indicating a good quality of the measurements according to the constraint of quasi-neutrality. The ion Larmor radius
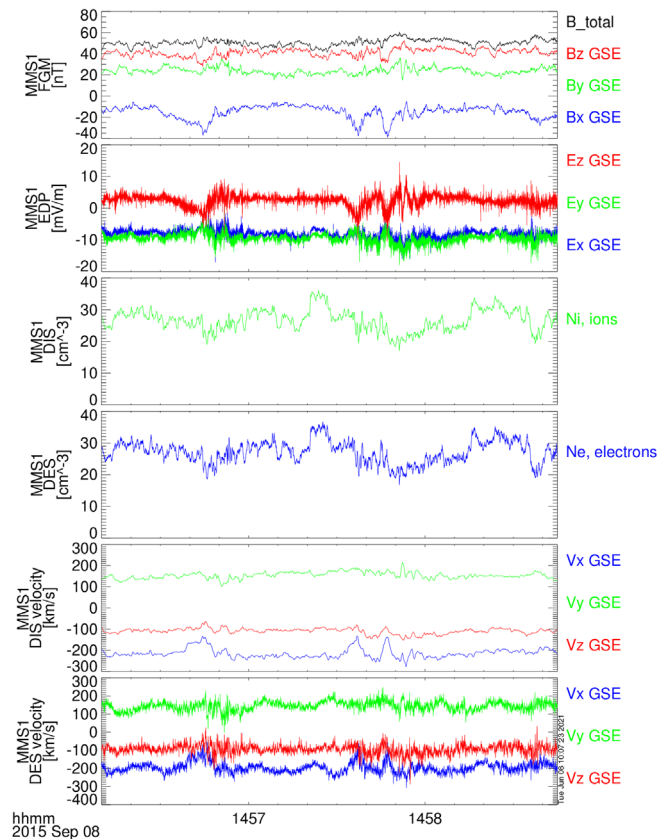


FIG. 1. Measured data from the MMS1 spacecraft. From top to bottom, the magnetic field from the fluxgate magnetometer, the electric field in the spacecraft frame from the spin plane double probes and the axial double probes, the ion density, the electron density, the ion velocity, and the electron velocity from the fast plasma investigation.

and the inertial lengths are 43.3 and 43.7 km/rad, respectively, Ion and electron plasma parallel plasma $\beta$ (the ratio of parallel thermal to magnetic pressure) are 0.61, 0.16, respectively.

To determine the wavevectors of the fluctuations in the plasma, we use two different, complementary methods. The first is the Multipoint signal resonator (MSR) technique[22] which is derived from wave-telescope/k-filtering methods.[23,24] This method assumes that the signal is weakly stationary and can be decomposed into a superposition of plane waves with a small component of incoherent noise. The main strength of this method is that multiple plane waves can be resolved at a single spacecraft frame frequency. The spatial scales accessible for investigation depend on the spacecraft separation with a Nyquist wavenumber of $k_{max} = \pi/\langle d \rangle$, where the angled brackets denote the average inter-spacecraft distance. We limit ourselves to a spacecraft frame frequency range between [0.1,1] Hz based on $k_{max}$ and the ion bulk speed. The other method used is Bellan's method;[25] where the strength of this method is that only a single spacecraft is necessary. Bellan's method uses the measured magnetic field, and the plasma current density from the particle measurements $\mathbf{J}(t) = nq(\mathbf{V_i}(t) - \mathbf{V_e}(t))$ where the ion data are interpolated onto the electron time tags. Here $n$ denotes the density (we use the electron density), $q$ denotes the fundamental unit of charge, $\mathbf{V_i}$, and $\mathbf{V_e}$ denote the ion and electron velocities, respectively. The wavevector is obtained as follows:

$$\mathbf{k}(\omega) = i\mu_0 \frac{\mathbf{J}(\omega) \times \mathbf{B}^*(\omega)}{\mathbf{B}(\omega) \cdot \mathbf{B}^*(\omega)}, \qquad (1)$$

where the $\omega$ in the parentheses denotes that these are complex amplitudes from the Fourier transform. The asterisk denotes the complex conjugate. For this study, we use the Bellan's method on each of the MMS spacecraft. Thus, the results presented are the mean of four independent measurements. Furthermore if one of the four wavevectors differ from the mean by an angle greater than 35°, we eliminate these points from our analysis.[26] Bellan's method also assumes that the fluctuations can be described as a plane wave and that there is only a single plane wave at each spacecraft frame frequency such that each frequency maps to a single wavevector. No such assumption is necessary for the MSR technique, where multiple wavevectors can be detected at a single spacecraft frame frequency. However, we only investigate the wavevector with the largest power from the MSR method. Another difference is the range of wavenumbers that are accessible for investigation. The range of wavenumbers that can be resolved by the MSR method is set by the inter-spacecraft distances. Whereas for Bellan's method, the limitation is from the length of the time series at large scales and the sampling rate/noise at small scales. The obtained wavevectors can then be used to obtain plasma frame frequencies according to the Doppler-shift relationship:

$$\omega_{pla} = \omega_{sc} - \mathbf{k} \cdot \langle \mathbf{V_i} \rangle. \qquad (2)$$

The $\omega_{pla} - k$ relation can then be compared with linear solutions of the Vlasov equation.

## III. RESULTS

Figure 2 shows the wavelet[27] power spectra of the trace magnetic field (using the Alfvén normalization to velocity units) (a), the trace electron velocity (b) the trace ion velocity (c), and the electron density (d). The vertical lines displayed on the spectra denote ion inertial length $d_i = V_A/\Omega_{ci}$, the ion gyroradius $\rho_i = v_{i\perp}/\Omega_{ci}$, and the
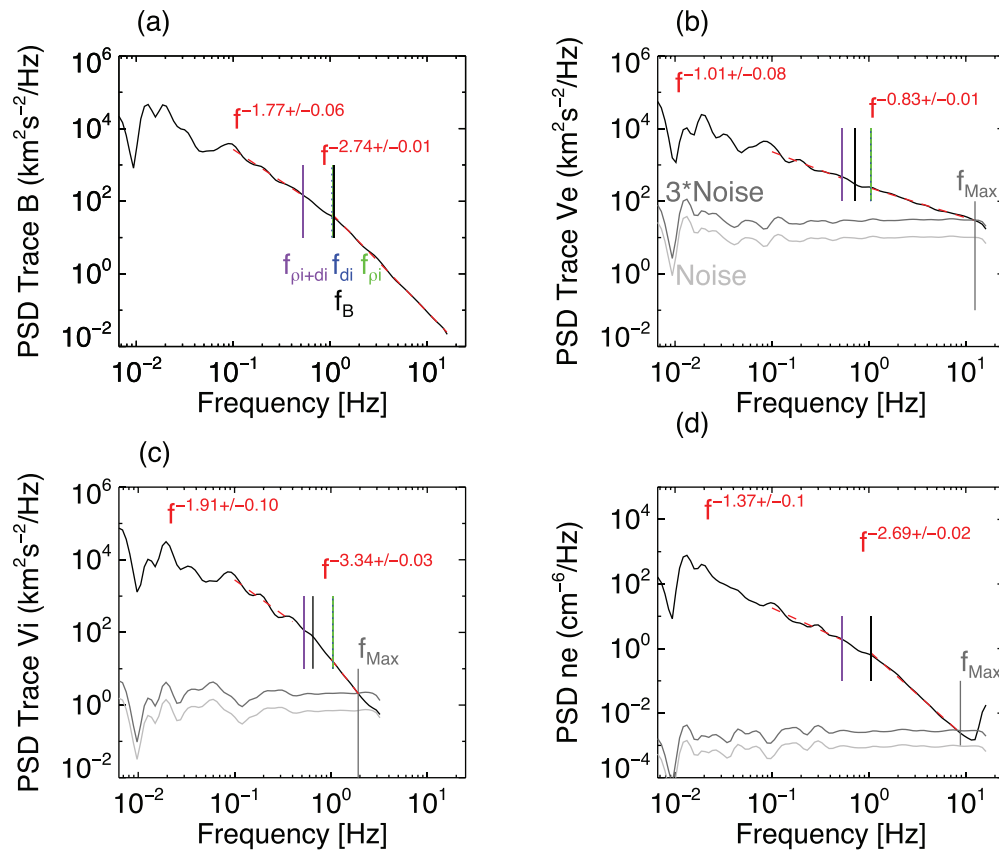
**FIG. 2.** Wavelet power spectrum of the trace magnetic field spectrum (a) the trace electron velocity spectrum (b), the trace ion velocity spectra (c), and the electron density spectrum (d). The vertical lines denote different ion scales, with purple denoting the combined scale, green denoting the ion inertial, and blue denoting the ion gyro scale. The black vertical lines denotes the intersection of the power-law fits between large and small scales. The gray curve denotes the estimated noise floor based on the statistical uncertainties,[26] and the dark gray curve denotes three times the noise floor, which is used to find the maximum reliable frequency.

combined scale $\rho_i + d_i$[28] which are expressed as Taylor shifted scale, e.g., $f_{d_i} = V_{bulk}/2\pi d_i$. The estimated noise floor of the measured quantities is also displayed along with the noise floor value multiplied by three for the ion velocity, the electron velocity, and the electron density. For the magnetic field, the noise floor is outside the plotting range; the other quantities of noise floors are determined from the statistical errors of the measurements given in the level 2 moments data on the MMS data archive. The errors are used to define a white noise signal, e.g., Gershman et al.[26] A maximum reliable frequency is defined here as the frequency where the measured value is equal to three times the estimated noise floor.[29]

At large scales above the Taylor shifted proton scales, it is difficult to determine the spectral index accurately as the interval is short and the cone of influence (COI) affects the results at large scales.[27] Consequently, there is only a limited range available to estimate the spectral index. We fit from a minimum value of 0.1 Hz (to limit the influence of the COI) up to the combined scale $f \sim 0.5$ Hz. At the smaller scales, we fit from the shifted ion inertial length scale to the maximum frequency $f_{Max}$, where $f_{Max}$ is different for each measurement. We choose these limits to avoid fitting over any of the relevant spatial scales. Furthermore, we avoid noise at small scales and the cone

of influence at large scales. The black line indicated as $f_B$ denotes the intersection of the two power-law fits. The magnetic field spectrum shows a typical steepening near the ion scales to an index near $\sim -2.6$ fairly typical in the solar wind and the magnetosheath.[6,7,30–33] At large scales $f < 0.2$ Hz, the ion and electron velocity spectra are similar. At these scales, both ions and electrons are magnetized and thus coupled in their motion. At smaller scales, the ion and electron velocity spectra begin to differ. The ion velocity spectra are much steeper at small scales $\sim -3.3$.[6,34,35] This is expected at these scales as the plasma leaves the MHD regime and ion-resonant dissipation sets in. The electron velocity spectrum is shallower than the ion velocity spectrum, and no clear break is observed. The density spectrum shows a similar slope to the magnetic spectrum at small scales, while at large scales, it is flatter. A flatter spectrum is often observed in the density in the solar wind forming a transition between the ion inertial and kinetic ranges and is sensitive to the $\beta$ value.[36–39] However, our time series' are not long enough to compare larger scales to confirm that this is indeed a flattening.

The predictions from linear theory for the kinetic Alfvén wave[10,40–43] and the ion Bernstein wave[44] are calculated from the New Hampshire Dispersion Solver[45] using the mean parameters from the

interval (plasma $\beta$, temperature anisotropy). The results are displayed in Fig. 3, column 1, for the Alfvén branch, and column 2 for the Ion Bernstein branch. The propagation directions used are $\theta_{kb} = 80°$ (dashed lines) and $\theta_{kb} = 89°$ (solid lines), which is motivated from the typical wavevector anisotropy $k_\perp \gg k_\parallel$ often observed in plasma turbulence[46–48] and the wavevector observations from the interval (which will be discussed later). Figures 3(a) and 3(b) show the real frequencies in black and the imaginary part of the frequency in red (i.e., the damping rate). The kinetic Alfvén wave (KAW) branch has low frequencies, while the ion Bernstein branch has much higher frequencies. However, we cannot distinguish between a quasi-perpendicular KAW and an advected structure (i.e., a spatial variation with $\omega_{pla} = 0$) using this methodology. The ambiguity comes from the uncertainty[48] and the natural fluctuations in the velocity[49] used for the Doppler shift [Eq. (2)]. Panel (c) displays the plasma frame frequency as a function of the wavenumber. The wavevector is determined from the MSR technique (blue) and Bellan's method (red). We apply the methods in the frequency range of 0.1–1 Hz in the spacecraft frame. This frequency range corresponds to the Nyquist wavenumber set by the mean inter-spacecraft distance. The spacecraft frame frequency is obtained according to Eq. (2). The obtained wavevectors make a quasi-perpendicular angle with the mean magnetic field direction $88 \pm 5°$ from the MSR method and $82 \pm 15°$ from Bellan's method (which justifies the propagation angles of the linear theory solutions). Bellan's method is applied to all four spacecraft and any wavevector which differs by an angle larger than $35°$ from the mean of all four is removed. Both methods produce consistent results, and fluctuations have low plasma frame frequencies compared to the cyclotron frequency except for one outlier in Bellan's method. The high frequency of this data point is likely due to more than one wavevector being
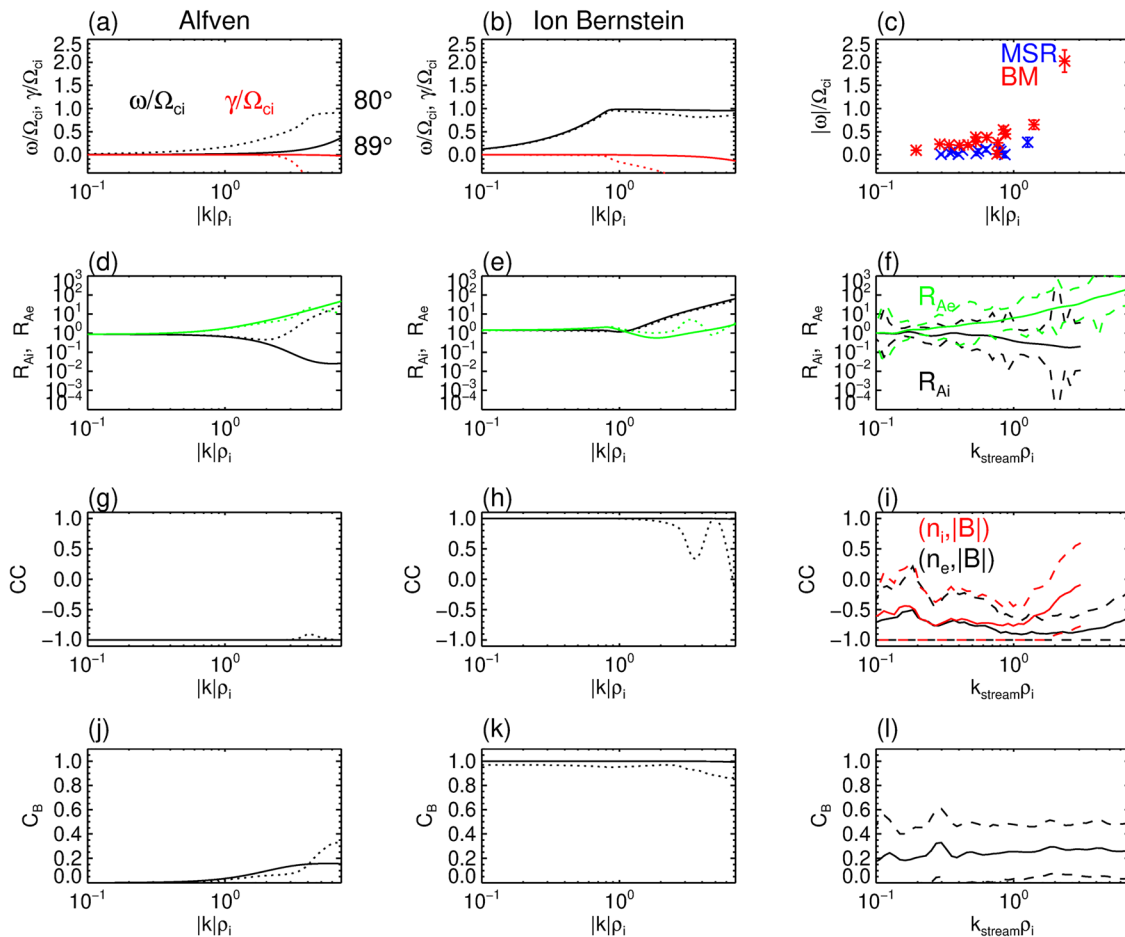


**FIG. 3.** The first two columns show the predictions of linear theory for a Kinetic Alfvén wave (column 1) and for an ion Bernstein wave (column 2). Panels (a) and (b) show the frequency, with the real part in black and the imaginary part in red. Solid lines denote a propagation angle of $89°$ and dashed lines denote an angle of $80°$. Panels (d) and (e) show the ion Alfvén ratio in black and the electron Alfvén ratio in green. Panels (g) and (h) show the cross correlation of density and compressive magnetic field. Panels (j) and (k) show the magnetic compressibility. Column 3 shows the observations from the MMS spacecraft. Panel (c) shows the dispersion relation diagram from the MMS data using the MSR data (blue) and Bellan method (red). Panel (f) shows the measured ion and electron Alfvén ratios (solid lines) and their relative errors (for display on logarithimc axis). Panel (i) shows the cross correlation of the density and magnetic field strength (solid lines), dashed lines denote the standard deviations. Panel (l) shows the compressibility (solid lines) and the standard deviations.

present for a given Fourier mode, which causes a large error in the Bellan method. However, the MSR method does not share this limitation and multiple wavevectors can be identified at a single frequency.

The second row denotes the ion (black) and electron (green) Alfvén ratios, which is the ratio of the trace velocity fluctuations to the trace magnetic fluctuations (in Alfvén units). The Alfvén ratio of species $j$ is given by

$$R_{A,j} = \mu_0 n m_i \frac{|\delta \mathbf{v}_j|^2}{|\delta \mathbf{B}|^2}. \quad (3)$$

For the observations in panel (f), these are converted to a wavenumber following Taylor's hypothesis for the spacecraft measurements (other than the plasma frame frequency). It is important to recall that converting to a wavenumber this way does not give the true wavenumber of the fluctuations; instead, it gives a streamwise wavenumber denoted $k_{stream} = 2\pi f / V_i$. Where the streamwise wavenumber is related to $k_\perp$ as $k_{stream} = k_\perp \sin(\theta_{BV})\cos(\phi)$, where $\phi$ is the angle between $\mathbf{k}$ and the $\mathbf{B}$ $\mathbf{V}$ plane. If anisotropy $k_\perp \gg k_\parallel$ is assumed (which is observed for this interval), then $k_\perp \simeq k$ and $\phi$ is small then it follows that $k_{stream} \simeq k\sin(\theta_{BV})$.[50] As $\theta_{BV} \simeq 80°$, the difference between $k$ and $k_{stream}$ is expected to be small. The prediction of the Alfvén ratio for large-scale Alfvén waves is 1, while for magnetosonic waves, it is $\sim$2, e.g., Gary.[51] For KAWs [panel (d)], near the ion gyrolength $k\rho_i \sim 1$ the ion and electron ratios begin to depart from one another. The magnetic field fluctuations' power become dominant over the ion velocity, while the electron velocity fluctuations' power becomes dominant. For the ion Bernstein wave [panel (e)], both ion and electron velocities are dominant. The observations in panel (f) which show a decrease in the ion Alfvén ratio with increasing wavenumber and an increase in the electron Alfvén ratio, which is more consistent with the predictions for kinetic Alfvén waves.

Row three denotes the cross correlation between the magnitude of the magnetic field and the density for species j, which is given by

$$CC = \frac{\Re(\delta n_j \delta |B|^*)}{|\delta n_j||\delta |B||}, \quad (4)$$

where the asterisk denotes the complex conjugate. The Alfvén solutions and the IBW solutions show anti-correlated and correlated fluctuations, respectively. The measurements show that the fluctuations are mostly anti-correlated throughout the ranges investigated, more consistent with the KAWs rather than the IBWs. In the final row, we see the magnetic compressibility defined as the fluctuations of the parallel component over the trace component,

$$C_B = \frac{|\delta B_\parallel|^2}{|\delta B_\parallel|^2 + |\delta B_{\perp 1}|^2 + |\delta B_{\perp 2}|^2}, \quad (5)$$

where the parallel component is defined as the component along the mean magnetic field direction calculated over the interval. Throughout the range, they have a value of roughly 0.3, again more consistent with the KAW solutions rather than the IBW.

To understand the potential mechanisms for dissipation, we calculate the resonance parameters following.[52,53] For a species $s$, the resonance condition is quantifiable by

$$\zeta = \frac{\omega_{pla} - m\Omega_s}{k_\parallel v_{s,thermal}}, \quad (6)$$

where $\Omega_s$ is the cyclotron frequency of species $s$ and $v_{s,thermal}$ is the thermal speed of species $s$, $m$ is an integer with $m = 0$ giving the condition for Landau resonance and $m = \pm 1$ giving the condition for the first cyclotron resonance, the parameters $k$ and $\omega_{pla}$ are determined from the MSR and Bellan's method, presented in Fig. 3(a). When $\zeta \approx 1$, then resonant energy transfer from the electromagnetic fields can occur efficiently. We note that our definition of $\zeta$ in Eq. (6) is based on the thermal speed, while the full velocity distribution of the particles provides an infinite range of velocities that can potentially resonate. Nevertheless, the thermal speed is appropriate for characterizing a significant number of particles that can efficiently resonate.[54] The mean values of the resonance parameters are presented in Table I. Both methods have consistent results and suggest that the ion and Landau resonances may be possible in the interval; however, for cyclotron resonance, $\zeta \gg 1$ for both ions and electrons.[52,53] For ion scales, we do not expect the electron cyclotron resonance to be active; this is reflected in the result that the resonance parameters are much larger than 1. Should we measure larger wavevectors which is possible for the smaller MMS separations, perhaps the electron cyclotron resonance becomes more important. The standard deviations are large for all cases. The large standard deviations are due to the difficulty in measuring the parallel wavenumber, which is small and can cause the resonance parameter to become very large as it is in the denominator of Eq. (6).

Figure 4 shows the evolution of the resonance parameters as a function of the wavenumber. The error bars denote the relative error of the resonance parameters. Note that some of the errors are large as the frequency measured is low in some cases which leads to a large relative error despite the absolute error being small. The dashed line indicates a resonance parameter of 1. Even considering the error bars, the resonance condition for either cyclotron resonance is not fulfilled. For the ion Landau resonance, the points are predominantly above 1 but some errors straddle and some points lie beneath the value of unity, indicating that ion Landau resonance could be occurring. For the electron Landau resonance, the points are all below 1 but in general show a trend toward 1. At smaller scales than studied here ($k\rho_i > 1.6$), it is possible that electron Landau damping becomes more important. Observations of magnetic spectra show steepening at roughly $5 > k\rho_i > 30$[31,32,46,55,56,61] which could be interpreted as being due to the onset of electron Landau damping.[57]

To further investigate Landau damping as a potential mechanism for the conversion of energy from the fields to the kinetic energies, we

**TABLE I.** The mean, the standard deviations, and the min/max values of the resonance parameter analysis.

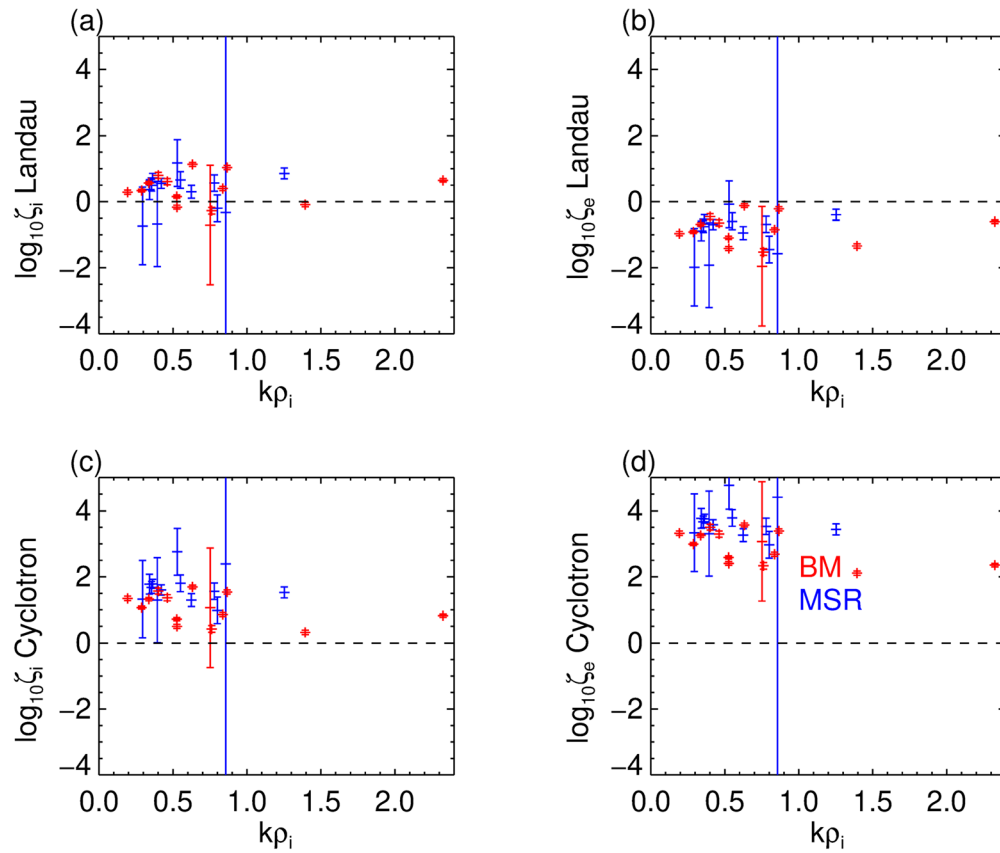|  | Mean | Standard deviation | Min | Max |
|---|---|---|---|---|
| Ion Landau (MSR) | 3.6 | 3.9 | 0.18 | 14.85 |
| Electron Landau (MSR) | 0.2 | 0.2 | 0.01 | 0.84 |
| Ion Landau (Bellan) | 3.7 | 3.9 | 0.19 | 13.44 |
| Electron Landau (Bellan) | 0.2 | 0.2 | 0.01 | 0.76 |
| Ion cyclotron (MSR) | 97 | 159 | 10 | 600 |
| Electron cyclotron (MSR) | 10 000 | 16 000 | 900 | 60 000 |
| Ion cyclotron (Bellan) | 17 | 15 | 2 | 50 |
| Electron cyclotron (Bellan) | 1400 | 1300 | 100 | 4000 |

**FIG. 4.** The resonance parameters as a function of wavenumber for the ion Landau resonance (a), the electron Landau resonance (b), the first ion cyclotron resonance (c), and the first electron cyclotron resonance (d). The error bars denote the relative error based on the propagation of the error on the plasma frame frequency.

investigate $\mathbf{J} \cdot \mathbf{E}'$.[58] Note that electric fields are frame dependent, so the measured spacecraft frame electric field needs to be transformed to the rest frame[59,60] using a mean measured velocity $\mathbf{E}' = \mathbf{E} + \langle \mathbf{V}_i \rangle \times \mathbf{B}$ (i.e., subtracting the convective electric field). Here, the mean ion bulk velocity vector is used, although both the mean electron and ion bulk flows are similar in this interval. The $\mathbf{J} \cdot \mathbf{E}'$ parameter is the work done on the particles by the electric field and quantifies the transfer of energy between the fields and the particle kinetic energy. This is not strictly speaking dissipation as the energy is transferred to the kinetic energy rather than the internal energy of the particles.[62,87]

To obtain a scale dependent measure of the energy conversion, we use an energy conversion rate[63,64] defined as

$$\epsilon_{ECR} = \frac{1}{4}(\tilde{\mathbf{J}} \cdot \tilde{\mathbf{E}}'^* + \tilde{\mathbf{J}}^* \cdot \tilde{\mathbf{E}}'), \tag{7}$$

where the tildes denote the wavelet coefficients of $\mathbf{J}$ and $\mathbf{E}'$ and the asterisk denotes the complex conjugate. The scale-dependent $\epsilon_{ECR}$ is shown for the perpendicular direction, and the parallel direction in Fig. 5 where the dashed lines denote the mean value, and the shaded region denotes the standard deviation. The energy conversion rate in the parallel direction is defined as

$$\epsilon_{ECR,\parallel} = \frac{1}{4}(\tilde{J}_\parallel \cdot \tilde{E}'^*_\parallel + \tilde{J}^*_\parallel \cdot \tilde{E}'_\parallel), \tag{8}$$

while in the perpendicular direction, it is defined as

$$\epsilon_{ECR,\perp} = \frac{1}{4}\left[ (\tilde{J}_{\perp 1} \cdot \tilde{E}'^*_{\perp 1} + \tilde{J}^*_{\perp 1} \cdot \tilde{E}'_{\perp 1}) + (\tilde{J}_{\perp 2} \cdot \tilde{E}'^*_{\perp 2} + \tilde{J}^*_{\perp 2} \cdot \tilde{E}'_{\perp 2}) \right]. \tag{9}$$

At large scales Fig. 5(a) $k\rho_i < 0.5$ there is a significant fluctuation in the perpendicular value of the energy conversion rate whereas the parallel component is close to zero [Fig. 5(b)]. The large variations in the perpendicular energy conversion rate are associated with large-scale velocity fluctuations, e.g., those at 14:57:40–14:58:00 (see Fig. 1).

To get a clearer view of the fluctuations near $k\rho_i \sim 1$ we re-plot Figs. 5(a) and 5(b), only between $k\rho_i = 0.5 - 7$ with a limited y-axis. Figure 5(d) shows that the parallel component of the energy conversion rate is positive, which is suggestive of Landau damping. The standard deviations are large, indicating a transfer of energy in both directions; however, the secular net transfer is from the fields to the particles. The mean value is close to zero in the perpendicular components but is negative at the larger scales.

## IV. DISCUSSION

The nature of the ion and electron Alfvén ratios shows a good match with the expectations from linear Vlasov theory for a KAW. Consistent with the observations of Roberts *et al.*[65] for the ion Alfvén
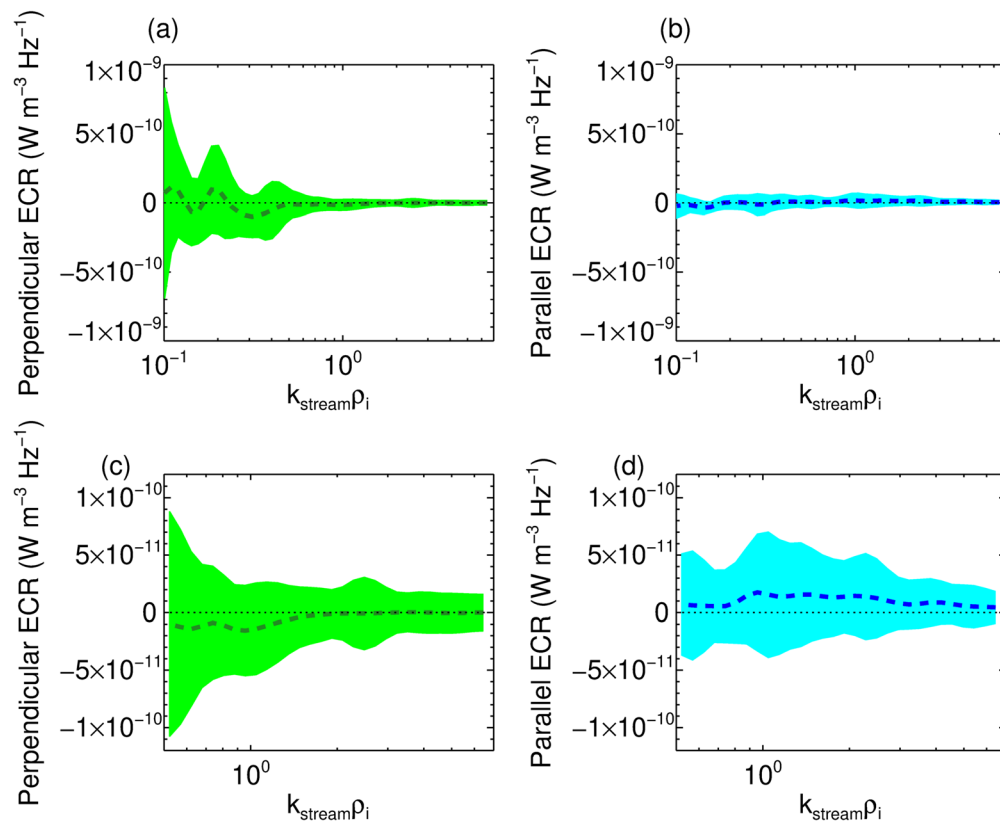
**FIG. 5.** Scale dependent energy conversion rate defined in Eq. (7) for the perpendicular components (a) and (c) and the parallel components (b) and (d).

ratio. We rule out the kinetic slow mode as its ion Alfvén ratio increases with increasing wavenumber.[66] The cross-correlations of density and magnetic field magnitude are also consistent with the KAW interpretation, as IBWs have the same positive correlations as MHD scale fast waves. Finally, the measured compressibility also matches the expectation for KAWs well. Kinetic slow waves and IBWs are expected to have $C_B \sim 1$. At scales $k\rho_i < 0.5$, the compressibility is larger than predicted for a KAW. The large compressibility is most likely due to fluid scale compressive coherent structures which have anti-correlated $n_e - B$ and similar Alfvénicities to KAWs but are more compressive. Possible structures could be compressive vortices, e.g.,[67] magnetic holes/mirror modes,[68] pressure balanced structures.[69,70] Kinetic slow waves could also contribute; however, they are typically strongly damped, although the low $\beta$ in this interval may allow them to exist longer than in high-$\beta$ intervals.

While we interpret the results by comparing them with linear wave solutions, it is possible that the fluctuations are not wave-like. After numerous wave-wave interactions due to the turbulent cascade, the frequency of a wave can be broadened[71,72] to be sideband waves[73,74] which do not necessarily correspond to a single wave as predicted from Vlasov theory.[75,76] Another possible wave interaction is the parametric instability[10,41,77] that can occur whenever the Alfvén wave interacts with a background density fluctuation. Even though the fluctuation level is $\delta B/B_0 = 0.15$ in our study, parametric instabilities are plausible

explanations to the observed data. Theoretical and numerical studies indicate that cross scale coupling[78] can occur and some of the daughter waves can propagate nearly perpendicular to the mean magnetic field.[77,79,80] The existence of three-wave couplings acting on the ion Bernstein waves is also indicated by the numerical study by.[81]

The results do suggest that Landau resonances of the ions and the electrons are more important than the cyclotron resonances consistent with the expectations of a kinetic Alfvén wave[10,40,42] and with a field-particle analysis of electrons carried out by Chen et al.[11] on a different magnetosheath interval. We note that the standard deviations of the resonance parameters is large, however considering the range of values the Landau resonances are likely more important than the cyclotron resonances in this interval. Further evidence of the importance of electron Landau damping comes from a wave-driven simulation of TenBarge et al.[82] which finds that heating in current sheets through the Landau resonance is more likely than Ohmic dissipation (due to the low collisionality).

Our results also suggest that ion Landau damping may be possible at these scales and electron Landau damping at smaller scales. A short variable 'transition range' is often observed in the solar magnetic field power spectrum between the inertial and the dissipation scales.[3,46,83] This has been interpreted as being due to ion Landau damping.[46] Although the resonance parameters are not equal to 1, the linear theory damping rates suggest that we are at slightly larger scales

than where we expect damping to occur for a linear KAW. Investigation of the parallel energy conversion rate also suggests that Landau damping is present at $k\rho_i > 0.5$.

To better understand the dissipation processes at various scales, numerous intervals should be analyzed with spacecraft separations near the different plasma scale lengths. It would be preferable to perform this with the same interval with multiple spacecraft.[84,85] Such a study is possible with multiple data intervals from the Cluster spacecraft or the MMS spacecraft. However, for MMS, the range of separations is relatively small, leading to a small number of time intervals with ion-scale separations.

## V. CONCLUSION

We have used the unique properties of MMS to reveal the properties of fluctuations near the ion kinetic scales in magnetosheath turbulence. The multiple spacecraft and the ability to measure the plasma current at high time resolutions enable the determination of the wavevector with two different approaches. The fluctuations at these scales have low plasma frame frequencies consistent with KAWs or advected structures that have no intrinsic frequency.

Other properties such as the ion and electron Alfvén ratios, cross-correlations between the compressive magnetic field, and magnetic compressibility agree well with the linear theory predictions for KAWs. However, as turbulence is an inherently nonlinear process, it is not apparent that these are signatures of waves in the classical sense. At larger scales ($k\rho_i \sim 0.1$), the compressibility is too large to be explained in terms of linear KAWs. Furthermore, there is energy transfer occurring in this range which is associated with regions with large scale fluctuations. Therefore, while the KAW interpretation is consistent with the results, it does not seem to be a complete description.

Finally, we remark that the measured resonance parameters suggest that in this interval at these scales, cyclotron resonance either with electrons or ions is not important. The resonance parameters and $\mathbf{J} \cdot \mathbf{E}'$ support that Landau resonance is important for the conversion of energy from the fields to kinetic energy in the magnetosheath.

## AUTHOR DECLARATIONS
### Conflict of Interest

The authors declare that the research was conducted in the absence of any commercial or financial relationships that could be construed as a potential conflict of interest.

## DATA AVAILABILITY

The data that support the findings of this study are openly available in the MMS data archive at https://lasp.colorado.edu/mms/sdc/public/, Ref. 86.

## REFERENCES

[1]C. Y. Tu and E. Marsch, "MHD structures, waves and turbulence in the solar wind: Observations and theories," Space Sci. Rev. **73**, 1–210 (1995).

[2]R. Bruno and V. Carbone, "The Solar Wind as a Turbulence Laboratory," Living Rev. Sol. Phys. **10**, 2 (2013).

[3]O. Alexandrova, C. H. K. Chen, L. Sorriso-Valvo, T. S. Horbury, and S. D. Bale, "Solar wind turbulence and the role of ion instabilities," Space Sci. Rev. **178**, 101–139 (2013).

[4]O. Alexandrova, "Solar wind vs magnetosheath turbulence and Alfvén vortices," Nonlinear Processes Geophys. **15**, 95–108 (2008).

[5]O. Alexandrova and J. Saur, "Alfvén vortices in Saturn's magnetosheath: Cassini observations," Geophys. Res. Lett. **35**, L15102, https://doi.org/10.1029/2008GL034411 (2008).

[6]C. H. K. Chen and S. Boldyrev, "Nature of kinetic scale turbulence in the Earth's magnetosheath," Astrophys. J. **842**, 122 (2017).

[7]L. Matteini, O. Alexandrova, C. H. K. Chen, and C. Lacombe, "Electric and magnetic spectra from MHD to electron scales in the magnetosheath," Mon. Not. R. Astron. Soc. **466**, 945–951 (2017).

[8]O. W. Roberts, Y. Narita, R. Nakamura, Z. Vörös, and D. Gershman, "Anisotropy of the spectral index in ion scale compressible turbulence: MMS observations in the magnetosheath," Front. Phys. **7**, 184 (2019).

[9]R. J. Stefant, "Alfven wave damping from finite gyroradius coupling to the ion acoustic mode," Phys. Fluids **13**, 440 (1970).

[10]A. Hasegawa and L. Chen, "Kinetic process of plasma heating due to Alfvén wave excitation," Phys. Rev. Lett. **35**, 370 (1975).

[11]C. H. K. Chen, K. G. Klein, and G. G. Howes, "Evidence for electron Landau damping in space plasma turbulence," Nat. Commun. **10**, 740 (2019).

[12]K. Osman, W. Matthaeus, A. Greco, and S. Servidio, "Evidence for inhomogeneous heating in the solar wind," Astrophys. J. **727**, L11 (2011).

[13]R. Bandyopadhyay, A. Chasapis, R. Chhiber, T. N. Parashar, W. H. Matthaeus, M. A. Shay, B. A. Maruca, J. L. Burch, T. E. Moore, C. J. Pollock, B. L. Giles, W. R. Paterson, J. Dorelli, D. J. Gershman, R. B. Torbert, C. T. Russell, and R. J. Strangeway, "Incompressive energy transfer in the Earth's magnetosheath: Magnetospheric multiscale observations," Astrophys. J. **866**, 106 (2018).

[14]D. Grošelj, C. H. K. Chen, A. Mallet, R. Samtaney, K. Schneider, and F. Jenko, "Kinetic turbulence in astrophysical plasmas: Waves and/or structures?," Phys. Rev. X **9**, 031037 (2019).

[15]O. W. Roberts, D. Verscharen, Y. Narita, R. Nakamura, Z. Vörös, and F. Plaschke, "Possible coexistence of kinetic Alfvén and ion Bernstein modes in sub-ion scale compressive turbulence in the solar wind," Phys. Rev. Res. **2**, 43253 (2020).

[16]J. L. Burch, T. E. Moore, R. B. Torbert, and B. L. Giles, "Magnetospheric multiscale overview and science objectives," Space Sci. Rev. **199**, 5–21 (2016).

[17]C. T. Russell, B. J. Anderson, W. Baumjohann, K. R. Bromund, D. Dearborn, D. Fischer, G. Le, H. K. Leinweber, D. Leneman, W. Magnes, J. D. Means, M. B. Moldwin, R. Nakamura, D. Pierce, F. Plaschke, K. M. Rowe, J. A. Slavin, R. J. Strangeway, R. Torbert, C. Hagen, I. Jernej, A. Valavanoglou, and I. Richter, "The magnetospheric multiscale magnetometers," Space Sci. Rev. **199**, 189–256 (2016).

[18]C. Pollock, T. Moore, A. Jacques, J. Burch, U. Gliese, Y. Saito, T. Omoto, L. Avanov, A. Barrie, V. Coffey, J. Dorelli, D. Gershman, B. Giles, T. Rosnack, C. Salo, S. Yokota, M. Adrian, C. Aoustin, C. Auletti, S. Aung, V. Bigio, N. Cao, M. Chandler, D. Chornay, K. Christian, G. Clark, G. Collinson, T. Corris, A. De Los Santos, R. Devlin, T. Diaz, T. Dickerson, C. Dickson, A. Diekmann, F. Diggs, C. Duncan, A. Figueroa-Vinas, C. Firman, M. Freeman, N. Galassi, K. Garcia, G. Goodhart, D. Guererro, J. Hageman, J. Hanley, E. Hemminger, M. Holland, M. Hutchins, T. James, W. Jones, S. Kreisler, J. Kujawski, V. Lavu, J. Lobell, E. LeCompte, A. Lukemire, E. MacDonald, A. Mariano, T. Mukai, K. Narayanan, Q. Nguyan, M. Onizuka, W. Paterson, S. Persyn, B. Piepgrass, F. Cheney, A. Rager, T. Raghuram, A. Ramil, L. Reichenthal, H. Rodriguez, J. Rouzaud, A. Rucker, Y. Saito, M. Samara, J.-A. Sauvaud, D. Schuster, M. Shappirio, K. Shelton, D. Sher, D. Smith, K. Smith, S. Smith, D. Steinfeld, R. Szymkiewicz, K. Tanimoto, J. Taylor, C. Tucker, K. Tull, A. Uhl, J. Vloet, P. Walpole, S. Weidner, D. White, G. Winkert, P.-S. Yeh, and M. Zeuch, "Fast plasma investigation for magnetospheric multiscale," Space Sci. Rev. **199**, 331–406 (2016).

[19]P.-A. Lindqvist, G. Olsson, R. B. Torbert, B. King, M. Granoff, D. Rau, G. Needell, S. Turco, I. Dors, P. Beckman, J. Macri, C. Frost, J. Salwen, A. Eriksson, L. Åhlén, Y. V. Khotyaintsev, J. Porter, K. Lappalainen, R. E. Ergun, W. Wermeer, and S. Tucker, "The spin-plane double probe electric field instrument for MMS," Space Sci. Rev. **199**, 137–165 (2016).

[20]R. E. Ergun, S. Tucker, J. Westfall, K. A. Goodrich, D. M. Malaspina, D. Summers, J. Wallace, M. Karlsson, J. Mack, N. Brennan, B. Pyke, P. Withnell, R. Torbert, J. Macri, D. Rau, I. Dors, J. Needell, P. A. Lindqvist, G. Olsson, and C. M. Cully, "The axial double probe and fields signal processing for the MMS mission," Space Sci. Rev. **199**, 167–188 (2016).

[21]P. Robert, A. Roux, C. Harvey, M. Dunlop, P. Daly, and K.-H. Glassmeier, "Tetrahedron geometric factors," in *Analysis Methods for Multi-Spacecraft Data*, edited by P. Paschmann and G Daly (1998), Chap. 13, pp. 323–348.

[22]Y. Narita, K.-H. Glassmeier, and U. Motschmann, "High-resolution wave number spectrum using multi-point measurements in space—The multi-point signal resonator (MSR) technique," Ann. Geophys. **29**, 351–360 (2011).

[23]J. Pincon and F. Lefeuvre, "Local characterization of homogeneous turbulence in a space plasma from simultaneous measurements of field components at several points in space," J. Geophys. Res. **96**, 1789–1802, https://doi.org/10.1029/90JA02183 (1991).

[24]U. Motschmann, T. I. Woodward, K. H. Glassmeier, D. J. Southwood, and J. L. Pinçon, "Wavelength and direction filtering by magnetic measurements at satellite arrays: Generalized minimum variance analysis," J. Geophys. Res.: Space Phys. **101**, 4961–4965, https://doi.org/10.1029/95JA03471 (1996).

[25]P. M. Bellan, "Revised single-spacecraft method for determining wave vector k and resolving space-time ambiguity," J. Geophys. Res. A **121**, 8589–8599, https://doi.org/10.1002/2016JA022827 (2016).

[26]D. J. Gershman, A. F. Viñas, J. C. Dorelli, M. L. Goldstein, J. Shuster, L. A. Avanov, S. A. Boardsen, J. E. Stawarz, S. J. Schwartz, C. Schiff, B. Lavraud, Y. Saito, W. R. Paterson, B. L. Giles, C. J. Pollock, R. J. Strangeway, C. T. Russell, R. B. Torbert, T. E. Moore, and J. L. Burch, "Energy partitioning constraints at kinetic scales in low-$\beta$ turbulence," Phys. Plasmas **25**, 022303 (2018).

[27]C. Torrence and G. P. Compo, "A practical guide to wavelet analysis," Bull. Am. Meteorol. Soc. **79**, 61–78 (1998).

[28]R. Bruno and L. Trenchi, "Radial dependence of the frequency break between fluid and kinetic scales in the solar wind fluctuations," Astrophys. J. **787**, L24 (2014).

[29]O. Alexandrova, J. Saur, C. Lacombe, A. Mangeney, S. J. Schwartz, J. Mitchell, R. Grappin, P. Robert, M. Maksimovic, K. Issautier, N. Meyer-Vernet, M. Moncuquet, and F. Pantellini, "Solar wind turbulent spectrum from MHD to electron scales," AIP Conf. Proc. **1216**, 144–147 (2010).

[30]C. W. Smith, K. Hamilton, B. J. Vasquez, and R. J. Leamon, "Dependence of the dissipation range spectrum of interplanetary magnetic fluctuationson the rate of energy cascade," Astrophys. J. **645**, L85–L88 (2006).

[31]O. Alexandrova, J. Saur, C. Lacombe, A. Mangeney, J. Mitchell, S. Schwartz, and P. Robert, "Universality of solar-wind turbulent spectrum from MHD to electron scales," Phys. Rev. Lett. **103**, 165003 (2009).

[32]O. Alexandrova, C. Lacombe, A. Mangeney, R. Grappin, and M. Maksimovic, "Solar wind turbulent spectrum at plasma kinetic scales," Astrophys. J. **760**, 121 (2012).

[33]S. Y. Huang, F. Sahraoui, X. H. Deng, J. S. He, Z. G. Yuan, M. Zhou, Y. Pang, and H. S. Fu, "Kinetic turbulence in the terrestrial magnetosheath: Cluster observations," Astrophys. J. **789**, L28 (2014).

[34]J. E. Stawarz, S. Eriksson, F. D. Wilder, R. E. Ergun, S. J. Schwartz, A. Pouquet, J. L. Burch, B. L. Giles, Y. Khotyaintsev, O. L. Contel, P. A. Lindqvist, W. Magnes, C. J. Pollock, C. T. Russell, R. J. Strangeway, R. B. Torbert, L. A. Avanov, J. C. Dorelli, J. P. Eastwood, D. J. Gershman, K. A. Goodrich, D. M. Malaspina, G. T. Marklund, L. Mirioni, and A. P. Sturner, "Observations of turbulence in a Kelvin-Helmholtz event on 8 September 2015 by the magnetospheric multiscale mission," J. Geophys. Res. **121**, 11,021–11,034, https://doi.org/10.1002/2016JA023458 (2016).

[35]O. W. Roberts, S. Toledo-Redondo, D. Perrone, J. Zhao, Y. Narita, D. Gershman, R. Nakamura, B. Lavraud, C. P. Escoubet, B. Giles, J. Dorelli, C. Pollock, and J. Burch, "Ion-scale kinetic Alfvén turbulence: MMS measurements of the Alfvén ratio in the magnetosheath," Geophys. Res. Lett. **45**, 7974–7984, https://doi.org/10.1029/2018GL078498 (2018).

[36]B. D. G. Chandran, E. Quataert, G. G. Howes, Q. Xia, and P. Pongkitiwanichakul, "Constraining low-frequency Alfvénic turbulence in the solar wind using density-fluctuation measurements," Astrophys. J. **707**, 1668–1675 (2009).

[37]C. H. K. Chen, G. G. Howes, J. W. Bonnell, F. S. Mozer, K. G. Klein, and S. Bale, "Kinetic scale density fluctuations in the solar wind," arXiv:1210.0127v1 (2012).

[38]O. W. Roberts, R. Nakamura, K. Torkar, Y. Narita, J. C. Holmes, Z. Vörös, C. Lhotka, C. P. Escoubet, D. B. Graham, D. J. Gershman, Y. Khotyaintsev, and P.-A. Lindqvist, "Sub-ion scale compressive turbulence in the solar wind: MMS spacecraft potential observations," Astrophys. J. Suppl. Ser. **250**, 35 (2020).

[39]O. W. Roberts, J. Thwaites, L. Sorriso-Valvo, R. Nakamura, and Z. Vörös, "Higher-order statistics in compressive solar wind plasma turbulence: High-resolution density observations from the magnetospheric multiscale mission," Front. Phys. **8**, 464 (2020).

[40]L. Chen and A. Hasegawa, "Plasma heating by spatial resonance of Alfvén wave," Phys. Fluids **17**, 1399–1403 (1974).

[41]A. Hasegawa and L. Chen, "Kinetic processes in plasma heating by resonant mode conversion of Alfven wave," Phys. Fluids **19**, 1924 (1976).

[42]J. Hollweg, "Kinetic Alfvén wave revisited," J. Geophys. Res. **104**, 811–819 (1999).

[43]Y. Narita, O. W. Roberts, Z. Vörös, and M. Hoshino, "Transport ratios of the kinetic Alfvén mode in space plasmas," Front. Phys. **8**, 166 (2020).

[44]I. Bernstein, "Waves in a plasma in a magnetic field," Phys. Rev. **109**, 10 (1958).

[45]D. Verscharen and B. D. G. Chandran, "NHDS: The new Hampshire dispersion relation solver," Res. Notes AAS **2**, 13 (2018).

[46]F. Sahraoui, M. L. Goldstein, G. Belmont, P. Canu, and L. Rezeau, "Three dimensional anisotropic k spectra of turbulence at subproton scales in the solar wind," Phys. Rev. Lett. **105**, 131101 (2010).

[47]Y. Narita, S. Gary, S. Saito, K.-H. Glassmeier, and U. Motschmann, "Dispersion relation analysis of solar wind turbulence," Geophys. Res. Lett. **38**, L05101 (2011).

[48]O. W. Roberts, X. Li, and B. Li, "Kinetic plasma turbulence in the fast solar wind measured by cluster," Astrophys. J. **769**, 58 (2013).

[49]Y. Narita, "Four-dimensional energy spectrum for space-time structure of plasma turbulence," Nonlinear Processes Geophys. **21**, 41–47 (2014).

[50]S. Bourouaine, O. Alexandrova, E. Marsch, and M. Maksimovic, "On spectral breaks in the power spectra of magnetic fluctuations in fast solar wind between 0.3 and 0.9 Au," Astrophys. J. **749**, 102 (2012).

[51]S. P. Gary, "Low-frequency waves on a high-beta collisionless plasma: Polarization, compressibility and helicity," J. Plasma Phys. **35**, 431–447 (1986).

[52]Y. Narita, E. Marsch, C. Perschke, K.-H. Glassmeier, U. Motschmann, and H. Comişel, "Wave–particle resonance condition test for ion-kinetic waves in the solar wind," Ann. Geophys. **34**, 393–398 (2016).

[53]Y. Narita, E. Marsch, C. Perschke, U. Motschmann, K. H. Glassmeier, and H. Comisel, "Corrigendum to 'Wave–particle resonance condition test for ion-kinetic waves in the solar wind,' published in Ann. Geophys., 34, 393–398, 2016," Ann. Geophys. **34** (2016).

[54]S. Gary, *Theory of Space Plasma Microinstabilities* (Cambridge University Press, 1993).

[55]F. Sahraoui, S. Y. Huang, G. Belmont, M. L. Goldstein, A. Rétino, P. Robert, and J. De Patoul, "Scaling of the electron dissipation range of solar wind turbulence," Astrophys. J. **777**, 15 (2013).

[56]O. W. Roberts, O. Alexandrova, P. Kajdič, L. Turc, D. Perrone, C. P. Escoubet, and A. Walsh, "Variability of the magnetic field power spectrum in the solar wind at electron scales," Astrophys. J. **850**, 120 (2017).

[57]G. Howes, J. TenBarge, W. Dorland, E. Quataert, A. Schekochihin, R. Numata, and T. Tatsuno, "Gyrokinetic simulations of solar wind turbulence from ion to electron scales," Phys. Rev. Lett. **107**, 035004 (2011).

[58]S. Zenitani, M. Hesse, A. Klimas, and M. Kuznetsova, "New measure of the dissipation region in collisionless magnetic reconnection," Phys. Rev. Lett. **106**, 195003 (2011).

[59]S. D. Bale, P. J. Kellogg, F. S. Mozer, T. S. Horbury, and H. Reme, "Measurement of the electric fluctuation spectrum of magnetohydrodynamic turbulence," Phys. Rev. Lett. **94**, 215002 (2005).

[60]C. H. K. Chen, A. Mallet, T. A. Yousef, A. Schekochihin, and T. Horbury, "Anisotropy of Alfvénic turbulence in the solar wind and numerical simulations," Mon. Not. R. Astron. Soc. **415**, 3219–3226 (2011).

[61]G. G. Howes, S. C. Cowley, W. Dorland, G. W. Hammett, E. Quataert, and A. A. Schekochihin, "A model of turbulence in magnetized plasmas: Implications for the dissipation range in the solar wind," J. Geophys. Res.: Space Phys. **113**, A05103 (2008).

[62]W. H. Matthaeus, "Turbulence in space plasmas: Who needs it?," Phys. Plasmas **28**, 032306 (2021).

[63]J. He, D. Duan, T. Wang, X. Zhu, W. Li, D. Verscharen, X. Wang, C. Tu, Y. Khotyaintsev, G. Le, and J. Burch, "Direct measurement of the dissipation rate spectrum around ion kinetic scales in space plasma turbulence," Astrophys. J. **880**, 121 (2019).

[64]J. He, X. Zhu, D. Verscharen, D. Duan, J. Zhao, and T. Wang, "Spectra of diffusion, dispersion, and dissipation for kinetic Alfvénic and compressive turbulence: Comparison between kinetic theory and measurements from MMS," Astrophys. J. **898**, 43 (2020).

[65]O. W. Roberts, Y. Narita, and C.-P. Escoubet, "Multi-scale analysis of compressible fluctuations in the solar wind," Ann. Geophys. **36**, 47–52 (2018).

[66]J. S. Zhao, Y. Voitenko, M. Y. Yu, J. Y. Lu, and D. J. Wu, "Properties of short-wavelength oblique Alfven and slow waves," Astrophys. J. **793**, 107 (2014).

[67]D. Perrone, O. Alexandrova, A. Mangeney, M. Maksimovic, C. Lacombe, V. Rakoto, J. C. Kasper, and D. Jovanovic, "Compressive coherent structures at ion scales in the slow solar wind," Astrophys. J. **826**, 196 (2016).

[68]J. Soucek and C. P. Escoubet, "Cluster observations of trapped ions interacting with magnetosheath mirror modes," Ann. Geophys. **29**, 1049–1060 (2011).

[69]S. Yao, J.-S. He, E. Marsch, C.-Y. Tu, A. Pedersen, H. Rème, and J. G. Trotignon, "Multi-scale anti-correlation between electron density and magnetic field strength in the solar wind," Astrophys. J. **728**, 146 (2011).

[70]D. Verscharen, E. Marsch, U. Motschmann, and J. Müller, "Kinetic cascade beyond magnetohydrodynamics of solar wind turbulence in two-dimensional hybrid simulations," Phys. Plasmas **19**, 022305 (2012).

[71]G. G. Howes and K. D. Nielson, "Alfvén wave collisions, the fundamental building block of plasma turbulence. I. Asymptotic solution," Phys. Plasmas **20**, 072302 (2013).

[72]Y. Narita, "Space–time structure and wavevector anisotropy in space plasma turbulence," Living Rev. Sol. Phys. **15**, 2 (2018).

[73]C. Perschke, Y. Narita, U. Motschmann, and K.-H. Glassmeier, "Multi-spacecraft observations of linear modes and sideband waves in ion-scale solar wind turbulence," Astrophys. J. **793**, L25 (2014).

[74]C. Perschke, Y. Narita, U. Motschmann, and K.-H. Glassmeier, "Observational test for a random sweeping model in solar wind turbulence," Phys. Rev. Lett. **116**, 125101 (2016).

[75]Y. Nariyuki and T. Hada, "Remarks on nonlinear relation among phases and frequencies in modulational instabilities of parallel propagating Alfvén waves," Nonlinear Processes Geophys. **13**, 425–441 (2006).

[76]G. G. Howes, "A dynamical model of plasma turbulence in the solar wind," Philos. Trans. R. Soc. A **373**, 20140145 (2015).

[77]A. F. Viñas and M. L. Goldstein, "Parametric instabilities of circularly polarized large-amplitude dispersive Alfvén waves: Excitation of parallel-propagating electromagnetic daughter waves," J. Plasma Phys. **46**, 107–127 (1991).

[78]J. Zhao, Y. Voitenko, D. J. Wu, and J. De Keyser, "Nonlinear generation of kinetic-scale waves by magnetohydrodynamic Alfvén waves and nonlocal spectral transport in the solar wind," Astrophys. J. **785**, 139 (2014).

[79]D. Verscharen, E. Marsch, U. Motschmann, and J. Müller, "Parametric decay of oblique Alfvén waves in two-dimensional hybrid simulations," Phys. Rev. E **86**, 027401 (2012).

[80]H. Comişel, Y. Narita, and U. Motschmann, "Multi-channel coupling of decay instability in three-dimensional low-beta plasma," Ann. Geophys. **37**, 835–842 (2019).

[81]T. G. Jenkins, T. M. Austin, D. N. Smithe, J. Loverich, and A. H. Hakim, "Time-domain simulation of nonlinear radiofrequency phenomena," Phys. Plasmas **20**, 012116 (2013).

[82]J. M. TenBarge and G. G. Howes, "Current sheets and collisionless damping in kinetic plasma turbulence," Astrophys. J. **771**, L27 (2013).

[83]F. Sahraoui, L. Hadid, and S. Huang, *Reviews of Modern Plasma Physics* (Springer, Singapore, 2020), Vol. 4, pp. 1–33.

[84]K. G. Klein, O. Alexandrova, J. Bookbinder, D. Caprioli, A. W. Case, B. D. G. Chandran, L. J. Chen, T. Horbury, L. Jian, J. C. Kasper, O. L. Contel, B. A. Maruca, W. Matthaeus, A. Retino, O. Roberts, A. Schekochihin, R. Skoug, C. Smith, J. Steinberg, H. Spence, B. Vasquez, J. M. TenBarge, D. Verscharen, and P. Whittlesey, "[Plasma 2020 Decadal] Multipoint measurements of the solar wind: A proposed advance for studying magnetized turbulence," arXiv:1903.05740 (2019).

[85]L. Dai, C. Wang, Z. Cai, W. Gonzalez, M. Hesse, P. Escoubet, T. Phan, V. Vasyliunas, Q. Lu, L. Li, L. Kong, M. Dunlop, R. Nakamura, J. He, H. Fu, M. Zhou, S. Huang, R. Wang, Y. Khotyaintsev, D. Graham, A. Retino, L. Zelenyi, E. E. Grigorenko, A. Runov, V. Angelopoulos, L. Kepko, K. J. Hwang, and Y. Zhang, "AME: A cross-scale constellation of cubesats to explore magnetic reconnection in the solar–terrestrial relation," Front. Phys. **8**, 89 (2020).

[86]MMS Team (2021). "MMS Science Data Centre," MMS Team. https://lasp.colorado.edu/mms/sdc/public/

[87]Matthaeus et al., Astrophys. J. **891**, 101 (2020).